

2,5-Dihydroxybenzoic acid: laser desorption/ionisation as a function of elevated temperature[☆]

W.E. Wallace^{a,*}, M.A. Arnould^a, R. Knochenmuss^b

^a National Institute of Standards and Technology, Gaithersburg, MD 20899-8541, USA

^b Novartis Institutes for Biomedical Research, CH-4056 Basel, Switzerland

Received 14 July 2004; accepted 16 November 2004

Available online 16 December 2004

Abstract

The temperature dependence of laser desorption/ionization (LDI) ion yields has been measured for 2,5-dihydroxybenzoic acid (2,5-DHB) single crystals from room temperature to 160 °C using time-of-flight (TOF) mass spectrometry. A steep rise in ion production occurs at 90 °C, achieving a maximum at 120 °C, then decreases sharply to a minimum at 140 °C, and returns to a second maximum at 150 °C. Above 160 °C, useful information could not be obtained because of rapid volatilization of the sample into the vacuum. The overall trend in ion production, but not some of the details, is well described by a recent two-step theory of the laser desorption/ionization process, which takes into account the temperature-dependent effects of plume expansion. Measuring the background vacuum composition with a quadrupole mass spectrometer residual gas analyzer (RGA) showed an increase in thermal desorption of 2,5-DHB starting at 90 °C and maximizing at 130 °C. The increased neutral production by thermal desorption is believed to be the cause of the decrease in LDI ion production due to reduced pooling probabilities for laser-excited 2,5-DHB molecules. Thermal dehydration, condensation, and decarboxylation increase the volume of gas released at high temperatures which also serve to decrease LDI ion production at elevated temperatures. Lastly, to confirm the mass spectrometry results, the thermal desorption of 2,5-DHB single crystals under vacuum was measured using a quartz-crystal microbalance (QCM). The onset of desorption was found to occur at 90 °C and the maximum desorption rate was found at 135 °C.

Published by Elsevier B.V.

Keywords: Crystal growth; Desorption; Gentisic acid; Laser desorption/ionisation (LDI); Matrix-assisted laser desorption/ionisation (MALDI); Mass spectrometry; Organic acid; Sublimation; Thermal desorption

1. Introduction

Since its demonstration in 1991 as a suitable matrix for matrix-assisted laser desorption/ionization (MALDI) mass spectrometry by Strupat et al. [1], 2,5-dihydroxybenzoic acid (2,5-DHB) has been the subject of many investigations of both its solid state and gas-phase physical–chemical properties [2–20]. In this regard, 2,5-DHB may be the most thoroughly studied of all MALDI matrices. In 1998, Schürenberg et al. [9] conducted experiments on the apparent MALDI flu-

ence threshold of this matrix from room temperature down to –100 °C. Using the typical nitrogen gas laser (337 nm wavelength), they found that the minimum laser fluence required to observe laser desorption/ionization (LDI) radical molecular ions increased from 74 J/m² to 90 J/m² as the temperature decreased from +20 °C to –100 °C. For desorbed neutral molecules (converted to radical molecular ions in the gas phase by photoionization with 248 nm laser radiation) the fluence required increased from 24 J/m² to 37 J/m². These observations were interpreted using a quasi-thermal model based on the Arrhenius equation with the temperature augmented by the addition of the heat imparted to the sample by the laser [3].

In recent work on the MALDI mass spectrometry of polyethylene [21–24], a mass limit of about 15,000 u is ob-

[☆] Official contribution of the National Institute of Standards and Technology, not subject to copyright in the United States of America.

* Corresponding author. Tel.: +1 301 9755886; fax: +1 301 9753928.

E-mail address: william.wallace@nist.gov (W.E. Wallace).

served, above which it proved impossible to get intact macromolecular polyethylene ions into the gas phase. One plausible explanation is that the highly crystalline nature of polyethylene prevented the disentanglement of single chains from their crystallites embedded in the MALDI matrix. By heating above the melting point of polyethylene, we hope to overcome the heat of crystallization and remove this impediment. To begin our work on MALDI at elevated temperatures, we decided to study the ablation and thermal desorption characteristics of a common MALDI matrix as a function of elevated temperature. We chose 2,5-DHB because of the extensive literature on it as a MALDI matrix and because of the work of Schürenberg et al. [9] on its ablation characteristics below room temperature.

In the present work, the laser-desorbed ion production was measured as a function of temperature from room temperature to 160 °C by time-of-flight (TOF) mass spectrometry. In addition, neutral molecules thermally desorbed into the vacuum were monitored by a quadrupole mass spectrometer residual gas analyzer (RGA). In a separate experiment, the thermal desorption of 2,5-DHB was measured using a quartz-crystal microbalance (QCM) housed in a vacuum bell jar. Heating was found to impose additional complexities on the laser desorption experiment not encountered in the previous study of sample cooling [9]. In particular, thermal desorption into the vacuum at temperatures above 50 °C proved to be so rapid that the dried drop sample preparation method was not suitable. Due to the large surface area of such samples, the sample lifetime in the instrument was only a few minutes at 50 °C, and less than 1 min at temperatures above 80 °C. This proved too short a time to produce reasonable LDI mass spectra. To overcome these experimental difficulties, single-crystal samples were employed. The lower surface-to-volume ratio of the single crystals as well as their flat planar surfaces offered a level of stability in vacuum necessary to perform LDI experiments at the higher temperatures.

To these experimental results, we apply the two-step theory of the LDI process developed by Knochenmuss [25,26]. In the first step, which occurs during or shortly after the nanosecond-scale laser pulse, primary ionization of matrix molecules occurs via exciton diffusion and pooling in the solid state and in gas-phase clusters of matrix molecules. In the second step, ion–molecule reactions occur in the expanding LDI plume [27]. The ion–molecule reactions that occur in the second stage can be described using equilibrium gas-phase thermodynamics under conditions of ample in-plume molecular collisions (e.g., at sufficient laser power). This crucial insight may explain matrix or analyte suppression effects where cation affinity would be the critical controlling factor and should be predictable by comparing the difference in Gibbs free energy for cationization between the different species present [10,26,28]. This model also provides good quantitative agreement with changes in laser pulse length and spot-size (each when the laser pulse is held at constant total energy), changes in matrix to analyte ratio, and with time-delayed two-laser pulse studies [25,26,29,30]. Heating of the

sample alters in-plume collision rates which, in turn, alters the LDI ion production which is reflected in the two-step theory.

2. Experimental

2.1. Single-crystal growth

2,5-DHB (Fluka, Milwaukee, WI) [31] was purified twice by dissolving 10 g in a mixture of 90 mL distilled water and 10 mL methanol and heated to 55 °C until the DHB dissolved. The mixture was placed in a freezer at –10 °C for 1.5 h leading to precipitation of purified DHB. The precipitated DHB was filtered and washed at room temperature with fresh solvent mixture. The purified compound was placed in a vacuum oven overnight at 110 °C. Single crystals were grown by dissolving 1 g of purified DHB in 20 mL of distilled water at 70 °C giving a concentration of 50 mg/mL. The vial was capped and the warm solution was placed in a water bath at 36 °C and allowed to stand overnight. The temperature of the water bath was reduced 1.5 °C/d for 14 d until the temperature reached 15 °C. The vials were removed from the water bath and the mother liquor was decanted from the crystals. The crystals were placed under vacuum at room temperature overnight and subsequently stored in a desiccator until use. The crystals were approximately 5 mm × 3 mm × 2 mm. The largest crystal facet was always used in the ablation experiments. This corresponds to the {1 0 0} face of the monoclinic benzoic-acid-type structure of 2,5-DHB [7,32].

2.2. Instrumentation

The experiments were conducted on a Comstock Inc. (Oak Ridge, TN) model RTOF-260 time-of-flight mass spectrometer. Sample ablation was performed with the typical nitrogen gas laser at 337 nm. This instrument has several important features. The sample is held at ground potential during laser ablation. The laser strikes the sample along the centerline of the time-of-flight mass separator axis with a lateral deviation of no more than 2 mm. After a delay of 8 μs, a potential of +500 V is applied to the sample plate which repels the (positive) ions through a distance of 1.5 cm to a grounded grid and into the field of the flight tube held at –5000 V. The long delay and gentle extraction allow for full plume development. The ion source and entrance to the TOF mass separator, originally designed for gas-phase ionization experiments, have a large ionization volume and wide acceptance angle, respectively. Atom Sciences Inc. (Oak Ridge, TN) has modified this mass spectrometer to allow resistive heating of the copper sample stage to 200 °C. The copper sample stage that is permanently affixed in the instrument has many times the mass of the removable copper sample holder onto which the single crystals are placed. In this way, the temperature of the sample stage is little affected by the introduction of the sample holder (typically at room temperature). The sample holder fits snugly on

four sides into the sample stage allowing for maximum heat transfer. Nevertheless, as with all high-vacuum experiments defining the surface temperature of the sample is difficult, especially in the case where sublimation is occurring as in these experiments. However, based on our complementary quartz crystal microbalance experiments (described below), we expect the sample surface temperature to be no more than 10 °C below the indicated temperature.

The instrument is also equipped with a Stanford Research Systems (Sunnyvale, CA) model RGA200 quadrupole mass spectrometer, with an electron impact ionization source. This residual gas analyzer was capable of measuring masses up to 200 u with 1 u resolution and down to partial pressures of 1.3×10^{-12} Pa (1×10^{-14} torr). The base pressure of the source measured by the RGA, located on a side port about 25 cm from the laser ablation spot, was approximately 1.3×10^{-4} Pa (1×10^{-6} torr) rising as high as 1.3×10^{-3} Pa (1×10^{-5} torr) at the height of neutral gas production. The distance of the RGA from the sample meant that gas pressure directly above the sample surface was not determined. Determining gas pressure above the surface on the length scale of the ablation plume (where gas-phase chemistry is expected to occur) would be very difficult and was not attempted. Single-crystal samples were mounted on the target using conductive silver paste adhesive. No sign of adhesive out gassing was seen in the RGA even at the highest sample temperatures.

Each LDI-TOF spectrum represents the sum of 100 laser shots taken at a laser repetition rate of 12 Hz and a digitizer time base of 2 ns. The energy per pulse at threshold where DHB ions could be TOF detected was 54 μ J. The crystal-to-crystal variation of the threshold (as discussed below) was of the order of $\pm 1 \mu$ J. The laser spot size was 2.5×10^{-3} cm². It should be noted that the laser beam was not conditioned to have equal intensity across its diameter; thus, defining a single, exact spot area was not possible. Based on threshold energies reported in the literature, this area is likely an overestimate. The threshold energy found for a given crystal at room temperature was kept constant throughout a temperature run. Flight times were of the order of tens of microseconds. The sample was removed and held at ambient temperature and pressure between measurements (to prevent excessive loss of sample due to sublimation) while the sample stage was heated to the next temperature in 20 °C increments to 60 °C and then 10 °C increments beyond and allowed to equilibrate before the next measurement. The sample on the sample holder was then inserted into the sample stage. Data taking was commenced less than 1 min later, and lasted no more than 5 min at each temperature. The uncertainty in base peak (137 u) area calculated from triplicate measurements using the standard deviation from three separate crystals at room temperature was 35%, from the same crystal but at three different spots was 20%, and from the same crystal at the same spot was 11%. The corresponding uncertainties in mass for the base peak were ± 0.04 u, ± 0.01 u, less than ± 0.01 u, respectively.

An Inficon Corporation (Syracuse, NY) model XTC quartz crystal microbalance was mounted in a rough-pumped

vacuum bell jar. Single crystals of 2,5-DHB were heated using thin resistive heating elements embedded in a polyimide film. The single crystals were placed directly on the polyimide surface of the heating element. Temperature was measured by a thermocouple placed on the heating element next to the single crystal. Under a vacuum of approximately 0.13 Pa (1×10^{-3} torr), thermal desorption was measured as the temperature was raised from 20 °C to 200 °C. This was done in order to ascertain at what temperature in vacuum DHB began to sublime and to insure that the sublimation increased monotonically with temperature. The temperature set point was increased in 5 °C increments; when the thermocouple reading reached the new temperature (typically less than 1 min), the set point was adjusted to the next increment of temperature.

3. Ion yield calculations

A recently developed model [25,26] was applied without modification. A set of differential equations for the generation, decay, and reaction of matrix excited states and ions are numerically integrated over time. Exciton pooling reactions are the primary source of ions in this model. Parameters determined in earlier work [25] were employed, except that the starting temperature of the sample and the laser absorption coefficient were varied. The DHB sublimation temperature was again taken to be 450 K (177 °C)[33]. Below this temperature, the sample is presumed to remain solid. Above it, the sample is presumed to vaporize and expand adiabatically into the vacuum. During the expansion the rates of the pooling and other reactions in the model are scaled by the collision rate. The key parameter for the expansion is the heat capacity ratio. For a gas consisting only of DHB, this would be 1.008. If the gas consisted only of a triatomic like CO₂, it would be 1.154. To account for partial decarboxylation or dehydration of DHB during desorption, an intermediate value of 1.05 was used. This model is individually and sequentially applied to layers of the sample extending downward from the surface to a depth where the absorbed laser energy is negligible.

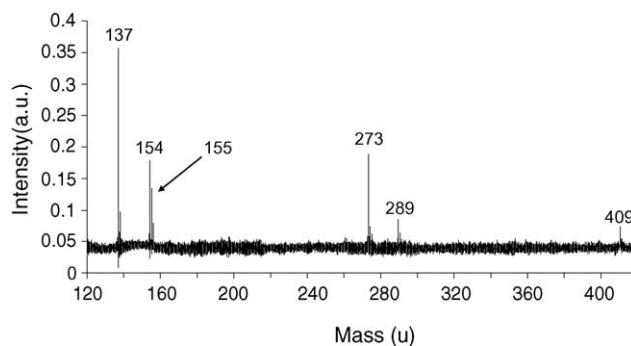


Fig. 1. Room temperature (20 °C) laser desorption/ionization time-of-flight mass spectrum from a 2,5-dihydroxybenzoic acid single crystal.

The stepwise picture of laser ablation obviously does not account for the continuous mass flux due to the elevated vapor pressure of the heated sample. However, only the material ejected as a direct result of the laser pulse is of interest for ion yields, since it contains the excited species which lead to ions. In addition, the vapor pressure of the solid prior to the laser pulse is small compared to that in the high-density material which is ejected during ablation. As a result, the model has been successful in describing physical aspects of the MALDI plume as well as ion yields [25].

4. Results

Fig. 1 shows a typical laser desorption/ionization time-of-flight (LDI-TOF) mass spectrum taken at slightly above the apparent threshold fluence from a 2,5-DHB single crystal held at room temperature. The base peak in the spectrum is the water-loss product $[\text{DHB} + \text{H} - \text{H}_2\text{O}]^+$ from protonated DHB (the oxonium ion) observed at 137 u. The peak observed at 154 u is the molecular ion

of DHB ($[\text{DHB}]^{\bullet+}$), while protonated DHB $[\text{DHB} + \text{H}]^+$ is observed at 155 u. The peak appearing at 273 u is a dimer formed by condensation/dehydration of DHB molecules (i.e., $[\text{2DHB} - 2\text{H}_2\text{O} + \text{H}]^+$), which can also be described as the protonated di-esterification product. A trimer can also be formed from the tri-esterification of DHB, $[\text{3DHB} - 3\text{H}_2\text{O} + \text{H}]^+$, and can be seen at 409 u. The peak at 156 u can be explained as $[\text{DHB} + 2\text{H}]^{\bullet+}$ while the peak at 289 u remains unidentified. Due to the small abundance of the peak at 156 u and the unknown origin of the peak at 289 u, neither was used in this study. It appears from Fig. 1 that at room temperature, the most abundant ions found in these experiments are those that result from dehydration (137 u) and condensation (273 u and 409 u). This statement is made based on the fact that the ions at 137 u and 273 u are more abundant than the molecular (154 u) and protonated (155 u) ions. Similar products and results have been observed in other studies where LDI was performed just above threshold irradiation [1,13]. Note the absence of sodiated [15] or potassiated [20] species (177 u and 193 u, respectively) in the spectrum which is a result of the purification step.

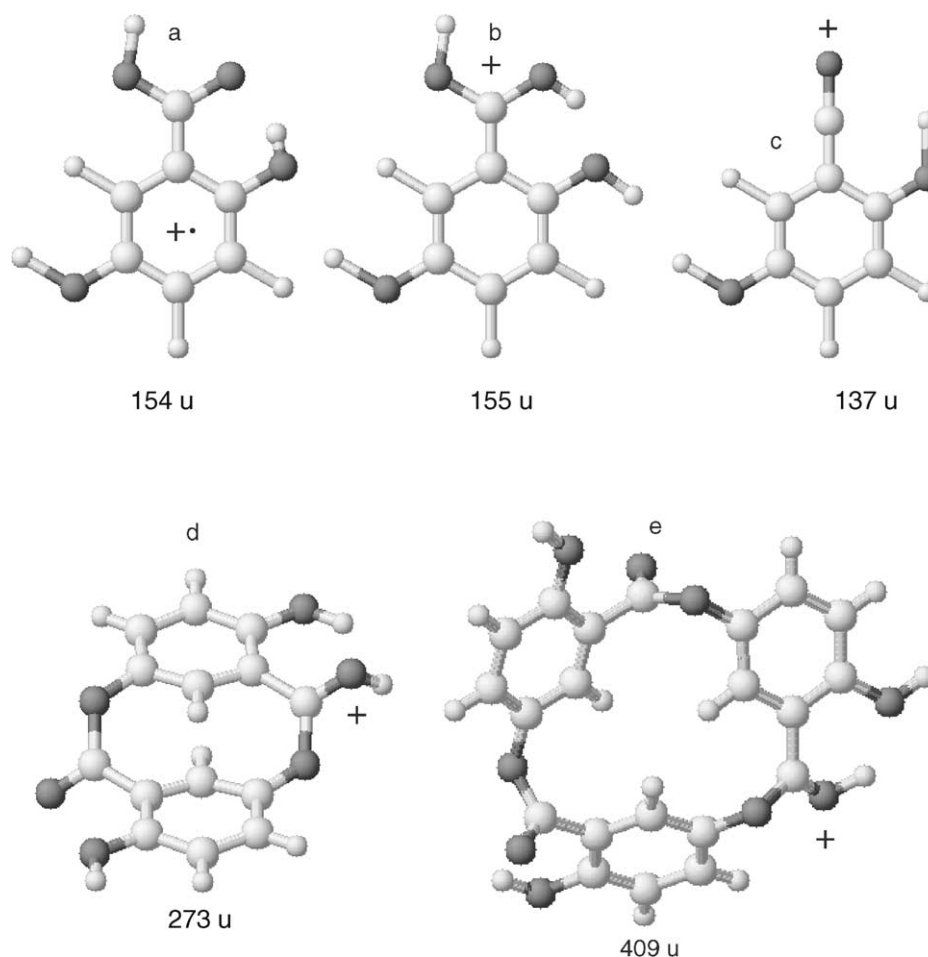


Fig. 2. Gas-phase structures for the most abundant species observed in Fig. 1. Calculated structures for (a) $[\text{DHB}]^{\bullet+}$ and (b) $[\text{DHB} + \text{H}]^+$ [13,14]. Hypothetical structures for (c) $[\text{DHB} + \text{H}^+ - \text{H}_2\text{O}]^+$ (oxonium ion), (d) $[\text{2DHB} - 2\text{H}_2\text{O} + \text{H}]^+$ (dimer formed from the condensation of 2 DHB molecules) and (e) $[\text{3DHB} - 3\text{H}_2\text{O} + \text{H}]^+$ (trimer formed from the condensation of 3 DHB molecules).

Fig. 2 shows the gas-phase structures for the most abundant species generated during the LDI experiment (Fig. 1). Structure a represents the optimized geometry for the molecular ion of DHB ($[\text{DHB}]^{\bullet+}$) with a distance between the carbonyl oxygen and the 2-hydroxy hydrogen in the range of 1.65–1.68 Å with either the radical cation delocalized in the aromatic benzene ring [13] or centered on the carbonyl oxygen [14] as calculated by Bourcier et al. using GAUSSIAN94. Structure b shows the optimized structure of DHB upon protonation ($[\text{DHB} + \text{H}]^+$) [13,14]. The distance between the proton on the carbonyl oxygen and the 2-hydroxy oxygen is 1.69 Å and the positive charge is delocalized on the carboxylic acid functionality [13,14]. The structures shown in c–e are hypothetical structures and have not been optimized by theory. The oxonium ion $[\text{DHB} + \text{H} - \text{H}_2\text{O}]^+$ is depicted by structure c and results from the fragmentation of protonated DHB (structure b). The positive charge resides on the oxygen which has a triple bond to the carbon. Structures d and e represent the hypothetical structures of the dimer ($[\text{2DHB} - \text{2H}_2\text{O} + \text{H}]^+$) and trimer ($[\text{3DHB} - \text{3H}_2\text{O} + \text{H}]^+$) of DHB that form upon the condensation of DHB molecules. This condensation can also be described as the di- or tri-esterification of DHB. The charged complexes result from the protonation of any of the carbonyl oxygens present in the macrocyclic ring. The condensation of more than three DHB molecules is not predicted due to the fact that the resulting structures would have unfavorable geometries resulting in ring strain. Larger cyclic ions are not observed, even at elevated temperatures.

A typical LDI-TOF mass spectrum from a single crystal held at 100 °C can be seen in the top panel Fig. 3. The difference between this spectrum and the one shown in Fig. 1 are limited to the intensities of the peaks at 137 u and 273 u. Upon comparison, the peaks observed at 154 u, 155 u and 409 u remain unaffected by the 80 °C temperature increase, while the peaks located at 137 u and 273 u, which represent fragment ions, increase two to three times in intensity. A typical spectrum from a single crystal held at 160 °C can be seen in the bottom panel Fig. 3. There is a further increase in the intensity of the peak at 137 u, a slight increase in the peak at 273 u and a complete loss of the cluster peak at 409 u. These spectra were taken at the same laser pulse energy as the room temperature spectrum shown in Fig. 1. It can be concluded that the deposition of energy from heating provides an increase in gas-phase DHB production upon laser ablation; however, from the results presented here, the gaseous molecules are more thermodynamically stable as fragment ions from either dehydration or condensation.

The results from the LDI of a single crystal of DHB as function of temperature can be seen in Fig. 4. Ion production profiles for the four major species observed in Figs. 1 and 3 are represented by lines plotted from the average of three temperature experiments (Fig. 4a–d). The uncertainties are those calculated from the standard error (the standard deviation divided by the square root of the number of experiments). The graphs in Fig. 4 do not represent absolute quantitation

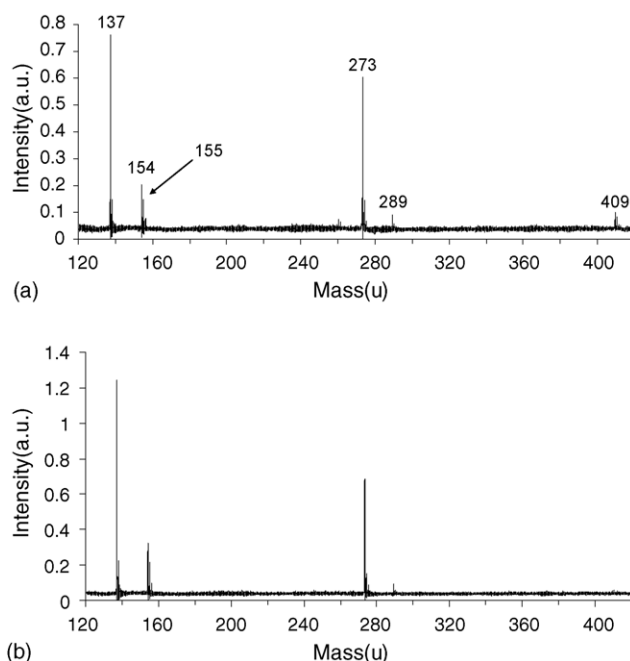


Fig. 3. (a) Laser desorption/ionization time-of-flight mass spectrum from a 2,5-dihydroxybenzoic acid (DHB) single crystal at 100 °C and (b) at 160 °C.

of ion production at any given temperature but instead represent trends in ion production. This is also true for similar plots that will be discussed later. The graphs show minor fluctuation in ion production from room temperature to 90 °C at which point fragment ion production (137 u and 273 u) increase dramatically to a maximum at 120 °C while the onset of intact DHB ion production (154 u and 155 u) begins at 110 °C reaching a maximum at 130 °C. Each type of ion reaches a local minimum at 140 °C; however, the $[\text{DHB} + \text{H}]^+$ at 155 u with its low ion intensity, this minimum is dominated by experimental uncertainty. This depression in ion production was consistently observed over more than a dozen single-crystal experiments. A second maximum for all ions can be observed at 150 °C. The decrease in ion production above 160 °C is due to rapid degradation of the crystal from heat and sublimation. By 160 °C, the crystal is so short lived that statistically meaningful mass spectra can be obtained only on the largest single-crystal samples. The reason of the large experimental uncertainty is that the absolute ion production varies dramatically from crystal to crystal at laser irradiation at just beyond threshold. The crystals appeared similar to the naked eye; however, subtle differences may affect the ion yields. It is this “crystal-to-crystal” variation that introduces uncertainty into the experiment and is hard to quantitate. The crystal-to-crystal variation includes: the thickness of the crystal (in particular, distance of the crystal surface from optimal laser focus point), surface imperfections (a rougher surface provides a larger surface area) and the angle of tilt relative to sample plate (altering the spot area and the amount of reflected light). A major difference between the two types of ions is in the amount produced by laser ablation. The amount

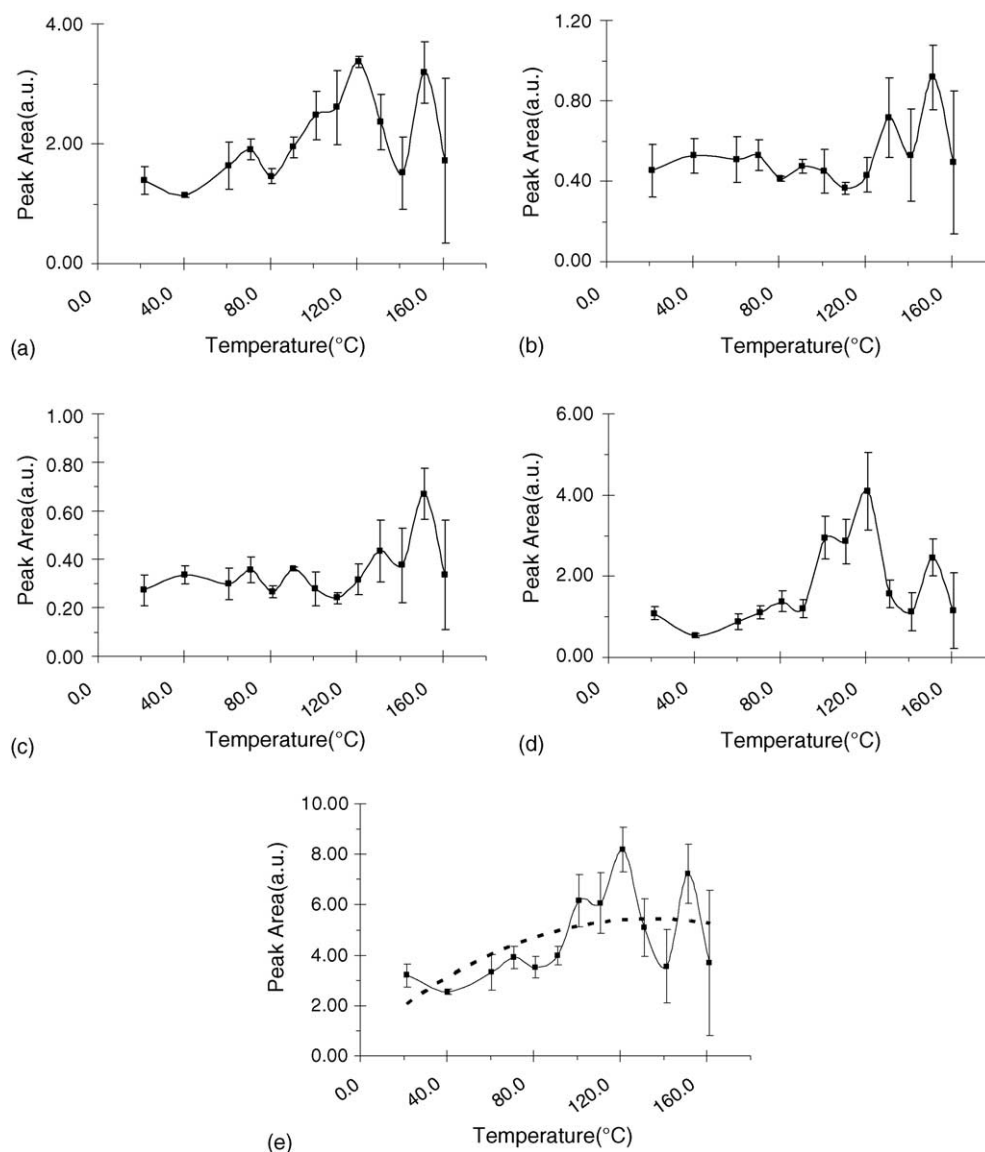


Fig. 4. Peak area as a function of temperature at constant fluence for the four major ions produced during laser ablation (a) 137 u, (b) 154 u, (c) 155 u and (d) 273 u. (e) The average of the summed peak areas for the triplicate analysis (average total ion production) fitted with a second-degree polynomial (---).

of fragment ions produced during LDI is consistently larger, even at lower temperatures, than the amount of intact DHB ions. The difference can be as large as an order of magnitude (Fig. 4a and d). This means that the summed ion curve is dominated by the behavior of the fragment ions.

The plot shown in Fig. 4e displays the sum of all four ion peak intensities as a function of temperature for all three temperature studies. This plot represents overall DHB ion production because the single crystal is the only source of analyte, keeping in mind that two peaks (289 u and 409 u) were not used in generating plots Fig. 4a–d. The plot is the average of these summed areas and is used to reveal the general trend. The trend in ion production behavior is readily observed here and there is no ambiguity in concluding that there is a significant decrease in ion production between 120 °C and 150 °C. Summing the peak areas at each temperature also dampens

the oscillation in the graph at lower temperatures revealing that the average increase in ion production does not begin until 90 °C.

A calculation of the DHB LDI ion yield versus initial temperature of the sample [25] is shown in Fig. 5a. The rounded shape of the curves shows that ion production reaches a maximum at elevated temperatures and then declines as temperature continues to increase. The curves were calculated using laser fluences believed to encompass the experimental values. The actual fluences are not easily determined due to inhomogeneity of the laser beam, the difficulty of measuring a representative spot diameter, and the variable focusing on crystals of different thickness. The absorption coefficient has a particularly large effect on these results since it linearly affects the energy deposited per unit volume. Higher absorption coefficient means that surface layers reach the sublimation tem-

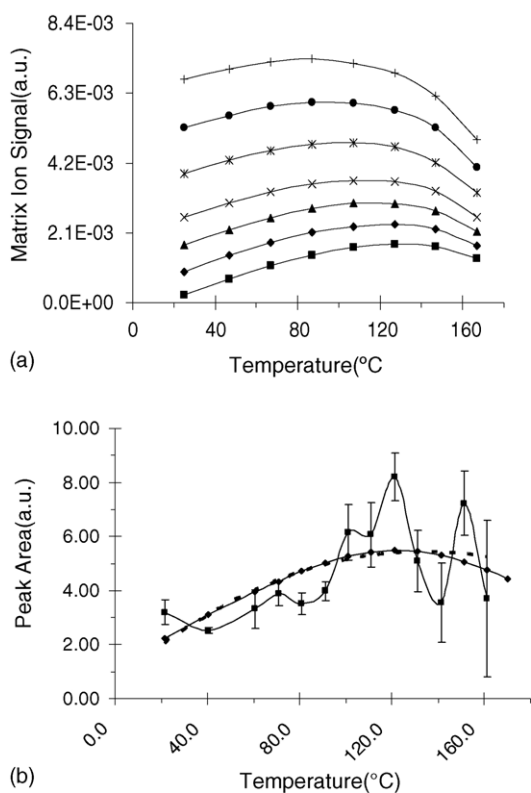


Fig. 5. (a) Calculation of the MALDI matrix ion yield from the two-step theory. The top four traces use an absorption cross-section of $3 \times 10^{17} \text{ cm}^2$ and the fluences were 9 mJ/cm^2 (+), 8 mJ/cm^2 (●), 7 mJ/cm^2 (Ж) and 6 mJ/cm^2 (×). The bottom three traces had an absorption cross section of $2 \times 10^{17} \text{ cm}^2$ and the fluences were 8 mJ/cm^2 (▲), 7 mJ/cm^2 (◆) and 6 mJ/cm^2 (■). (b) The average of the summed peak areas for the triplicate analysis fitted with a second-degree polynomial (---) with the theoretical result from the model using a fluence of 7 mJ/cm^2 and an absorption cross section of $2 \times 10^{17} \text{ cm}^2$ (◆) superimposed on the data after scaling for best fit.

perature sooner, but deeper layers do not reach it at all. This changes the peak temperature, mass density versus time, and ion yield considerably. Variations in behavior throughout the depth of the sample are averaged out to a certain degree, but Fig. 5 shows that important differences remain as a function of absorption coefficient. Plots for two values ($2 \times 10^{17} \text{ cm}^2$ and $3 \times 10^{17} \text{ cm}^2$) are shown in the figure, reflecting the experimental uncertainty for the coefficient in the solid state [34,35]. Fig. 5b shows the average of the summed peak areas from the triplicate analysis, a second-degree polynomial fitted to the data, and one result for the model calculation. This quadratic functional form was chosen because it, by definition, will possess a single maximum and, thus, should have a shape quite similar to the ion yield calculations. The model results that gave the best χ^2 fit to the data was for an absorption cross section of $2 \times 10^{17} \text{ cm}^2$ and a laser energy of 7 mJ/cm^2 . The fact that this is for a low absorption value and laser energy suggests that the experimental results were indeed carried out just beyond threshold. In Fig. 5b, it can be seen that the fitted model results almost exactly overlay the quadratic fit to the data.

Fig. 6a–d shows the 70 eV electron impact ionization (EI) ion intensities as a function of temperature for 2,5-DHB thermally desorbed into the vacuum taken using the quadrupole residual gas analyzer. The peaks at 80 u, 108 u, 136 u and 154 u are the fragment ions having the structures $[\text{DHB} - \text{H}_2\text{O} - 2\text{CO}]^{\bullet+}$, $[\text{DHB} - \text{H}_2\text{O} - \text{CO}]^{\bullet+}$, $[\text{DHB} - \text{H}_2\text{O}]^{\bullet+}$, and $[\text{DHB}]^{\bullet+}$, respectively. The four ions that are monitored in Fig. 6 are the fragments commonly observed upon EI at 70 eV [13,36]. Fig. 6e shows a graph of the triplicate sum of the intensity of the four fragments at each temperature. Plotting the sum of the four fragments is possible due to the fact that the fragments all originate from the same source, neutral DHB, and can be treated as the total amount of gaseous neutral DHB in the source. From Fig. 6e, it can be concluded that there is a significant increase in the thermally desorbed DHB (gaseous neutrals) from 100 °C similar to the increase observed in the LDI-TOF experiments (Fig. 4e). The plot also shows that neutral production maximizes at 130 °C before returning to a minimum at 150 °C followed by an increase beyond 150 °C. It is the maximum at 130 °C that holds the most interest. Upon comparison with Fig. 4e, it can be seen that the maximum of neutral production occurs exactly in the same temperature range as the minimum of the LD created ions.

Fig. 7 shows thermal desorption by mass as a function of temperature by quartz-crystal microbalance measurement. Again, the amount desorbed shows little change until 90 °C where there is a rapid rise in the deposition rate (Fig. 7a) and the thickness of material deposited on the QCM (Fig. 7b). It is important to note that the maximum in Fig. 7a coincides with the maximum of neutral production in the instrument (Fig. 6e) and the minimum of LDI ion production (Fig. 4e). This confirms the temperature range at which sublimation of DHB is at its greatest (130 °C). The dramatic decrease observed in Fig. 7a at 145 °C is largely due to the exhaustion of the crystal sample, although it should be noted that in most cases crystalline material was left on the polyimide film beyond 150 °C. Thus, beyond about 140 °C, the results of Fig. 7 should be treated with caution. Previous studies have suggested that DHB single crystals grown from water-containing solutions may contain entrained water [37,38]; however, no drastic changes in desorption rate or thickness were seen between 100 °C and 120 °C where entrained water may be expected to boil. As was the case in the mass spectrometry experiments, the sample is substantially lost above 160 °C, well before its 205 °C melting point [11].

5. Discussion

5.1. Model versus experimental results

The model well reproduces the general trend of the data (excluding the dip near 140 °C, discussed below). Ion yield slowly rises to a maximum then falls off more steeply. This

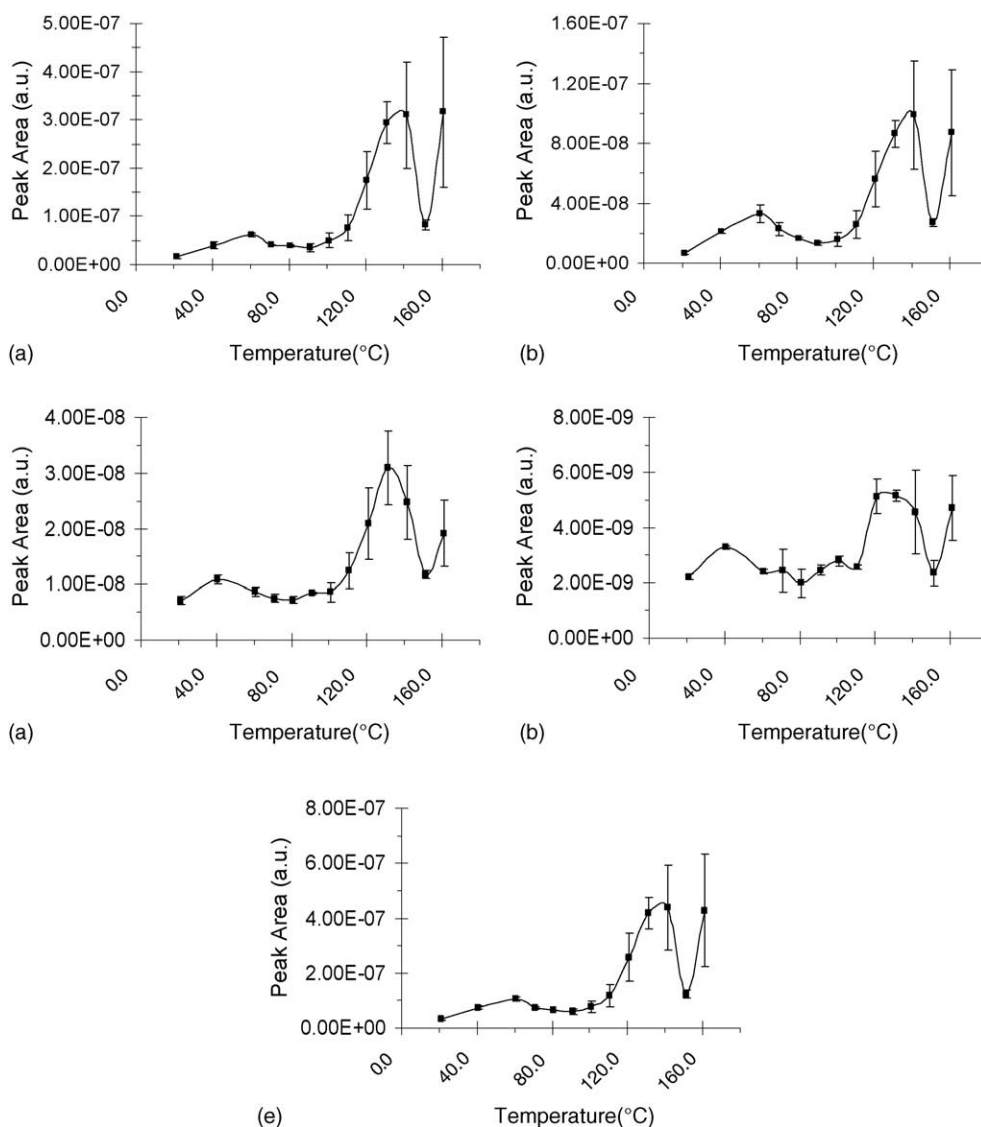


Fig. 6. Ion production from the 70 eV electron impact ionization (EI) of gas-phase DHB neutral molecules generated as a function of temperature. (a) $[\text{DHB} - \text{H}_2\text{O} - 2\text{CO}]^{\bullet+}$ (80 u), (b) $[\text{DHB} - \text{H}_2\text{O} - \text{CO}]^{\bullet+}$ (108 u), (c) $[\text{DHB} - \text{H}_2\text{O}]^{\bullet+}$ (136 u) and (d) $[\text{DHB}]^{\bullet+}$ (154 u). (e) The average of the summed areas for the triplicate analysis or average total neutral production.

shape is determined by competition between total ion production and losses from recombination. The initial rise at the lower temperatures primarily reflects reduced losses. In this region, ion generation is faster than vaporization, so total production is relatively constant. On the other hand, quicker release of ions by more rapid plume expansion at rising temperature reduces the extent of recombination, increasing yield.

In the upper temperature range where the ion yield begins to drop, ion production becomes limited by the speed of vaporization. Ionization by pooling is density dependent, so a sufficiently rapid vaporization and expansion can attenuate ion generation before it would normally finish. This is the origin of the drop in yield at the upper end of the temperature range studied.

The high-temperature yield dip is not predicted by the model, but is believed to be consistent with the principles governing yield outlined above. The model assumes a smoothly increasing amount of vaporized material versus input laser energy. It also assumes that the sample is vaporized only by the laser, into a vacuum which does not limit or modify the plume expansion. As shown in Fig. 6, these conditions are probably not met over the temperature range studied.

The ion yield minimum occurs at or near the substrate temperature where non-laser induced vaporization reaches its maximum. In this range, it is clear that incremental addition of laser energy to the sample will increase sample vaporization much more than at lower temperatures. As at the upper end of the calculated curve, this reduces net yield. In addition, the

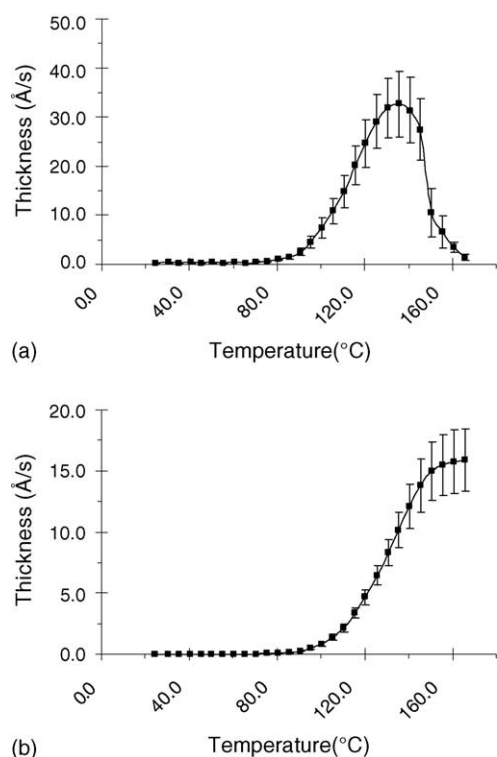


Fig. 7. Quartz crystal microbalance measurements of the sublimation of DHB into vacuum at elevated temperatures showing the (a) deposition rate and the (b) and the total deposited thickness.

plume expands into a DHB vapor that may be dense enough to reduce the extent of plume expansion or its rate. Again this favors recombination and a lower net yield. Finally, it is possible that the large amount of DHB vapor in the chamber at this temperature may absorb or scatter a significant fraction of the incoming laser pulse. Since MALDI is a non-linear effect, this will manifest itself as a disproportionate decrease in yield.

6. Conclusions

The laser desorption/ionization ion intensities have been measured for 2,5-dihydroxybenzoic acid single crystals from room temperature to 160 °C. A steep rise in total ion intensity occurs at 90 °C, peaks at 100 °C, decreases at 120 °C, and returns to a high value at 140 °C. Above about 150 °C, useful information could not be obtained due to the rapid thermal desorption of the sample into the vacuum. The overall trend in ion production, but not all the details, are well described by a two-step theory of the laser desorption/ionization process. The effects of a more rapid plume expansion from heated samples is the central consideration in predicting the overall increase in LDI ion yields. Following the background vacuum composition with a residual gas analyzer showed an increase in thermal desorption at 90 °C. The RGA results were confirmed by measuring thermal desorption by mass as a function

of temperature using a quartz-crystal microbalance confirming that the onset of increased LDI-TOF signal was largely due to increased sample sublimation.

References

- [1] K. Strupat, M. Karas, F. Hillenkamp, *Int. J. Mass Spectrom. Ion Processes* 111 (1991) 89.
- [2] B. Spengler, V. Bökelmann, *Nucl. Instrum. Methods Phys. Res. B* 82 (1993) 379.
- [3] K. Dreisewerd, M. Schürenberg, M. Karas, F. Hillenkamp, *Int. J. Mass Spectrom. Ion Processes* 141 (1995) 127.
- [4] K. Dreisewerd, M. Schürenberg, M. Karas, F. Hillenkamp, *Int. J. Mass Spectrom. Ion Processes* 154 (1996) 171.
- [5] D.A. Allwood, R.W. Dreyfus, I.K. Perera, P.E. Dyer, *Rapid Commun. Mass Spectrom.* 10 (1996) 1575.
- [6] J. Kampmeier, K. Dreisewerd, M. Schürenberg, K. Strupat, *Int. J. Mass Spectrom. Ion Processes* 169–170 (1997) 31.
- [7] K. Strupat, J. Kampmeier, V. Horneffer, *Int. J. Mass Spectrom. Ion Processes* 169–170 (1997) 43.
- [8] R.J.J.M. Steenvoorden, K. Breuker, R. Zenobi, *Euro. J. Mass Spectrom.* 3 (1997) 339.
- [9] M. Schürenberg, K. Dreisewerd, S. Kamanabrou, F. Hillenkamp, *Int. J. Mass Spectrom. Ion Processes* 172 (1998) 89.
- [10] K. Breuker, R. Knochenmuss, R. Zenobi, *Int. J. Mass Spectrom.* 184 (1999) 25.
- [11] D.M. Price, S. Bashir, P.R. Derrick, *Thermochim. Acta* 327 (1999) 167.
- [12] Q. Lin, R. Knochenmuss, *Rapid Commun. Mass Spectrom.* 15 (2001) 1422.
- [13] S. Bourcier, S. Bouchonnet, Y. Hoppilliard, *Int. J. Mass Spectrom.* 210–211 (2001) 59.
- [14] S. Bourcier, Y. Hoppilliard, *Int. J. Mass Spectrom.* 217 (2002) 231.
- [15] J. Zhang, T.K. Ha, R. Knochenmuss, R. Zenobi, *J. Phys. Chem. A* 106 (2002) 6610.
- [16] I. Fournier, C. Marinach, J.C. Tabet, G. Bolbach, *J. Am. Soc. Mass Spectrom.* 14 (2003) 893.
- [17] S.A. Pshenichnyuk, N.L. Asfandiarov, V.S. Fal'ko, V.G. Lukin, *Int. J. Mass Spectrom.* 227 (2003) 259.
- [18] Y. Chen, A. Vertes, *J. Phys. Chem. A* 107 (2003) 9754.
- [19] S.N. Jackson, S. Mishra, K.K. Murray, *J. Phys. Chem. B* 107 (2003) 13106.
- [20] J. Zhang, E. Dyachokva, T.K. Ha, R. Knochenmuss, R. Zenobi, *J. Phys. Chem. A* 107 (2003) 6891.
- [21] B.J. Bauer, W.E. Wallace, B.M. Fanconi, C.M. Guttman, *Polymer* 42 (2001) 9949.
- [22] R. Chen, T. Yalcin, W.E. Wallace, C.M. Guttman, L. Li, *J. Am. Soc. Mass Spectrom.* 12 (2001) 1186.
- [23] S. Lin-Gibson, L. Brunner, D.L. Vanderhart, B.J. Bauer, B.M. Fanconi, C.M. Guttman, W.E. Wallace, *Macromolecules* 35 (2002) 7149.
- [24] T. Yalcin, W.E. Wallace, C.M. Guttman, L. Li, *Anal. Chem.* 74 (2002) 4750.
- [25] R. Knochenmuss, *J. Mass Spectrom.* 37 (2002) 867.
- [26] R. Knochenmuss, *Anal. Chem.* 75 (2003) 2199.
- [27] R. Knochenmuss, A. Stortelder, K. Breuker, R. Zenobi, *J. Mass Spectrom.* 35 (2000) 1237.
- [28] R. Knochenmuss, R. Zenobi, *Chem. Rev.* 103 (2003) 441.
- [29] R. Knochenmuss, A. Vertes, *J. Phys. Chem. B* 104 (2000) 5406.
- [30] E. Moskovets, A. Vertes, *J. Phys. Chem. B* 106 (2002) 3301.
- [31] The identification of any commercial product or trade name does not imply endorsement or recommendation by the National Institute of Standards and Technology.
- [32] M. Haisa, S. Kashino, S. Hanada, K. Tanaka, S. Okazaki, M. Shibagaki, *Acta. Cryst. B38* (1982) 1480.

- [33] E. Stevenson, K. Breuker, R. Zenobi, *J. Mass Spectrom.* 35 (2000) 1035.
- [34] D.A. Allwood, P.E. Dyer, R.W. Dreyfus, *Rapid Commun. Mass Spectrom.* 11 (1997) 499.
- [35] K. Dreisewerd, *Chem. Rev.* 103 (2003) 395.
- [36] <http://webbook.nist.gov/chemistry/>.
- [37] E.E. Durrant, R.S. Brown, 50th American Society for Mass Spectrometry Conference on Mass Spectrometry and Allied Topics, 2002, Abstract A021223.
- [38] R. Krüger, A. Pfenninger, I. Fournier, M. Glückmann, M. Karas, *Anal. Chem.* 73 (2001) 5812.